RESEARCH ARTICLE

Key Points:
- First study of Callisto's magnetic environment including contributions from its plasma interaction and induction within its subsurface ocean
- Induction dominates the magnetic environment in a "core region" of Callisto's wake; plasma interaction dominates farther from the moon
- Comprehensive knowledge of ambient plasma conditions is required to adequately refine existing constraints on Callisto's subsurface ocean

Correspondence to:
L. Liuzzo,
lucas.liuzzo@eas.gatech.edu

Disentangling plasma interaction and induction signatures at Callisto: The Galileo C10 flyby

Lucas Liuzzo[1], Sven Simon[1], Moritz Feyerabend[2], and Uwe Motschmann[2,3]

[1] School of Earth and Atmospheric Sciences, Georgia Institute of Technology, Atlanta, Georgia, USA, [2] Institute for Theoretical Physics, University of Braunschweig, Braunschweig, Germany, [3] Institute for Planetary Research, German Aerospace Center, Berlin, Germany

Abstract We apply a combination of data analysis and hybrid modeling to study Callisto's interaction with Jupiter's magnetosphere during the Galileo C10 flyby on 17 September 1997. This encounter took place while Callisto was located near the center of Jupiter's current sheet. Therefore, induction in Callisto's subsurface ocean and magnetospheric field line draping around the moon's ionosphere both made nonnegligible contributions to the observed magnetic perturbations. The induction signal during C10 was obscured by plasma currents to a significant degree, in contrast to previously studied Callisto flybys. Our analysis reveals that at large distances to Callisto, its magnetic environment was dominated by field line draping, leading to the formation of Alfvén wings. Closer to the surface and in Callisto's wake, Galileo encountered a quasi-dipolar "core region" that was partially shielded from the plasma interaction and was dominated by the induced field. When exiting this core region, the spacecraft crossed a rotational discontinuity where the magnetic field vector rotated by approximately 50°. The hybrid model is able to quantitatively explain numerous key features of the observed magnetic signatures, especially the transitions between draping- and dipole-dominated regimes along the C10 trajectory. The model also reproduces the electron number density enhancement by 3–4 orders of magnitude detected in Callisto's wake, requiring a substantial ionosphere to surround the moon during C10. For flybys with nonnegligible plasma currents, comprehensive knowledge of the incident flow conditions and properties of Callisto's atmosphere is required to refine existing constraints on the subsurface ocean (conductivity, thickness, and depth) based on magnetic field data. These findings are highly relevant for the upcoming JUpiter ICy moon Explorer (JUICE) mission, which will include multiple Callisto flybys.

1. Introduction

Callisto, the second largest of the four Galilean moons, orbits in the equatorial plane of Jupiter at a distance of 26.3 R_J (radius of Jupiter $R_J = 71{,}492$ km). The 9.6° offset between the planet's rotation and magnetic axes causes the moon to experience a time-varying background magnetic field as it orbits. This time variability of the magnetospheric field induces currents within Callisto's conducting subsurface ocean, which generate a quasi-dipolar secondary magnetic field outside of the moon [*Kivelson et al.*, 1999; *Zimmer et al.*, 2000].

As Jupiter revolves, plasma rotating nearly synchronously with Jupiter continuously overtakes Callisto, thereby interacting with the moon's ionosphere [*Kliore et al.*, 2002] and the induced magnetic field from within its interior. This interaction leads to deceleration and deflection of the ambient flow due to mass loading of the magnetospheric plasma and causes magnetospheric field line draping, generating Alfvén wings [*Neubauer*, 1980, 1998]. Additionally, the moon's induced magnetic field is compressed at its ramside and stretched into a tail at its wakeside.

Although qualitatively similar processes occur at all four Galilean moons, Callisto is unique in its plasma interaction with the Jovian magnetosphere. Unlike the three inner Galilean moons (Io, Europa, and Ganymede) where the gyroradii of pickup ions are much smaller than the moons' radii, the ions composing Callisto's ionosphere have gyroradii up to 10 times its radius of $R_C = 2410$ km [*Liuzzo et al.*, 2015]. These large gyroradii result in a highly asymmetric plasma interaction, characterized by uneven magnetic pileup at Callisto's ramside and nonuniform flow shear between light and heavy ion species extending into the moon's wake [*Liuzzo et al.*, 2015]. Additionally, the thermal gyroradii of the incident magnetospheric ions are also comparable to the size of the moon [*Kivelson et al.*, 2004]. Callisto's plasma interaction therefore cannot be treated in the fluid regime.

The tilt of Jupiter's magnetic moment with respect to its spin axis causes Callisto to experience constantly varying plasma and magnetic environments. On the one hand, when Callisto is located near the Jovian magnetospheric current sheet, the ambient magnetospheric field is antialigned with the Jovian spin axis with a magnitude of approximately 4 nT [*Kivelson et al.*, 2004]. In this regime, the plasma interaction between Callisto and the Jovian magnetospheric plasma dominates the magnetic field perturbations near the moon [*Strobel et al.*, 2002]; i.e., it is much stronger than the induction signal from Callisto's interior. On the other hand, when Callisto is far above or below the Jovian current sheet and embedded within one of the giant planet's magnetodisk lobes, the background magnetospheric field can be an order of magnitude larger than in the current sheet and points radially toward or away from Jupiter. In this scenario, Callisto's interaction with the dilute magnetospheric plasma is weakened, and induced magnetic fields from its subsurface ocean dominate the near-Callisto magnetic environment. However, nearly 20% of the magnetic signatures near Callisto may still be generated by the plasma interaction [*Liuzzo et al.*, 2015], suggesting a mutual, nonlinear coupling between the two effects.

Over the course of the Galileo spacecraft's 8 year tour of the Jovian system (1995–2003), its magnetometer was active during seven flybys of Callisto. During the first two Callisto encounters (C3 on 4 November 1996 and C9 on 25 June 1997), the currents generated by the plasma interaction were weak, and the moon's magnetic environment was therefore dominated by the induction signal [*Khurana et al.*, 1998]. However, during the five remaining flybys (C10, C21, C22, C23, and C30), ambient currents driven by the plasma interaction with Callisto's ionosphere and induced dipole (i.e., the Pedersen, Hall, and Alfvénic current systems) were nonnegligible and partially obscured the induction signal [*Kivelson et al.*, 1999; *Zimmer et al.*, 2000]. Given the large size of the ion gyroradii compared to Callisto, the discrimination between plasma interaction and induction effects is particularly challenging. As a result, magnetic field and plasma data from Callisto encounters other than C3 and C9 have not yet been subject to successful modeling attempts. In other words, there is currently no method available to extract induction signatures from Callisto's magnetic environment when the plasma interaction concurrently generates nonnegligible contributions to the observed magnetic perturbations.

To close this gap, we present the first study of Callisto's magnetic and plasma environment that simultaneously considers the contributions of both the effect of Callisto's ionosphere and the effect of the induced dipole to the overall plasma interaction at the moon. In particular, our study focuses on modeling and analysis of magnetic field and plasma data obtained during the C10 wakeside encounter of Callisto on 17 September 1997. During this flyby, the magnetic perturbations generated by the plasma interaction with the moon's ionosphere and induced dipole field were comparable in strength to those signatures generated by induction in the moon's subsurface ocean alone. The major aim of this study is to identify those regions near Callisto where the magnetic field perturbations are dominated either by the moon's plasma interaction or by currents induced in its subsurface ocean. Using the C10 flyby as an example, we demonstrate how information about Callisto's conducting ocean can be extracted from magnetic field data collected during close flybys when the plasma interaction and induction both influence its magnetic environment. Similar studies of the entangled plasma interaction and induction process have been performed for flybys of the other three Galilean moons (for example, recently by *Rubin et al.* [2015] at Europa) but never before for a Callisto encounter. Thus, for the first time, this study proposes a strategy to discriminate between the individual contributions to Callisto's asymmetric and entangled magnetic environment.

This paper is structured as follows: first, a brief discussion of the C10 flyby is given in section 2, followed by an overview of the simulation model setup and the parameters used for the modeling component of our study (section 3). Section 4 presents the results of our study, including model comparison to Galileo flyby data and a discussion of our findings. Section 5 concludes the work, with outlook for the application of these findings to other Callisto flybys, specifically C21.

2. The C10 Flyby of Callisto

To study the C10 encounter of Callisto, the Cartesian CphiO coordinate system is used, in which the moon is centered at the origin. The axes of the system are defined such that magnetospheric corotation is along the x axis, the y axis points toward Jupiter, and the z axis is aligned with the Jovian spin axis. Throughout the study, unit vectors along these axes are denoted as $\hat{\mathbf{x}}$, $\hat{\mathbf{y}}$, and $\hat{\mathbf{z}}$, respectively.

The C10 flyby occurred when Callisto was approximately $3\,R_J$ south of the center of Jupiter's current sheet [*Kivelson et al.*, 1999] and located near 05:00 local time in its orbit around Jupiter [see *Liuzzo et al.*, 2015,
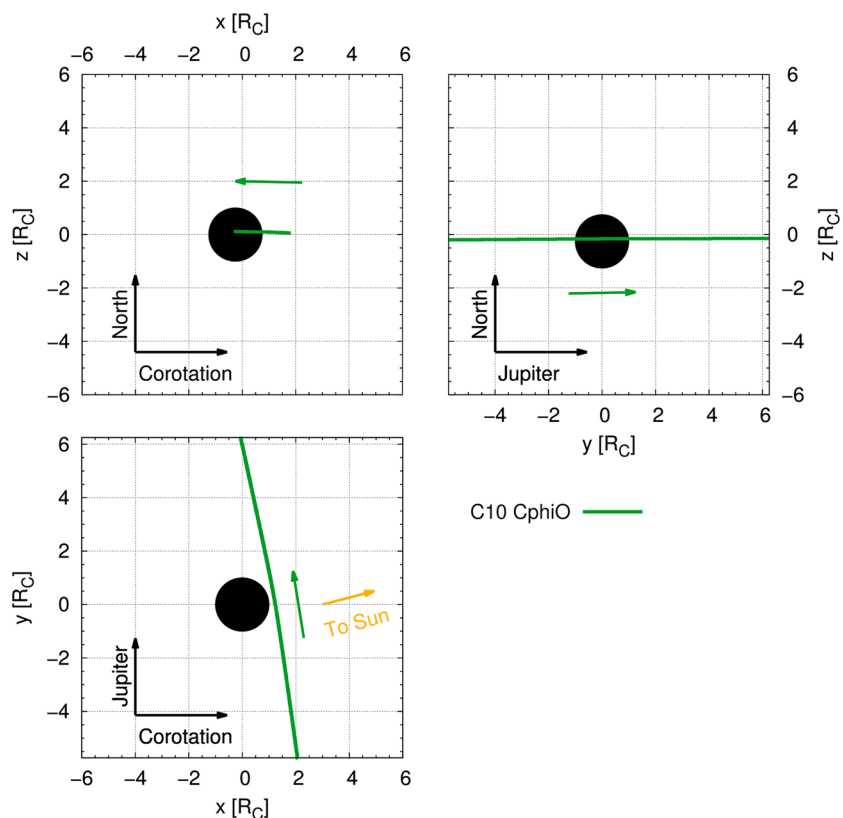
Figure 1. Projection of the C10 flyby trajectory onto the (top left) $y = 0\,R_C$, (top right) $x = 0\,R_C$, and (bottom left) $z = 0\,R_C$ planes. The trajectory is shown in green, and arrows denoting the direction of travel are included. The orange arrow in the $z = 0$ plane denotes the direction to the Sun. The Callisto-centered CphiO coordinate system is used (see text). The radius of Callisto is $R_C = 2410$ km.

Figure 1b]; i.e., the moon's wakeside hemisphere was almost completely illuminated, while its ramside hemisphere was dark. Galileo's trajectory during the encounter is shown in Figure 1. The spacecraft was nearly confined to Callisto's equatorial plane ($z = 0$), with a maximum vertical distance of $\Delta z = -0.11\,R_C$ to this plane. Galileo passed downstream of Callisto and spent 10 min in the moon's geometric *plasma* shadow defined by $\sqrt{y^2 + z^2} \leq R_C$ and $x > 0$. For simplicity, this region is referred to as *Callisto's geometric shadow* throughout. Note that this term *does not* refer to Callisto's *optical* shadow, which extended toward upstream during the flyby.

Traveling from the Jupiter-averted to the Jupiter-facing hemisphere of Callisto, Galileo's trajectory during C10 was slightly inclined toward upstream, forming an angle of 11.6° with the y axis. This geometry caused the spacecraft to reach its closest approach (C/A) to Callisto on 17 September 1997 at 00:18:55, at an altitude of 535.3 km ($0.22\,R_C$) in the Jupiter-facing ($y > 0$) hemisphere of the moon.

Only limited data from the C10 flyby are available in the literature. These include time series of the magnetic field [*Kivelson et al.*, 1999] and the number density of cold ionospheric electrons in Callisto's wake [*Gurnett et al.*, 2000]. However, the parameters of the incident magnetospheric plasma during the encounter (i.e., composition, density, velocity, and temperature) have not been presented in the literature. Additionally, radio occultation measurements of the ionosphere were not possible during C10, as the trajectory of the flyby and the orbital position of the moon were unfavorable. We will use this limited set of data to construct a plausible picture of Callisto's plasma interaction region during the C10 flyby.

3. Model Description

In contrast to the other three Galilean moons, the large gyroradii at Callisto require ions to be treated in the kinetic picture. This study therefore applies the Adaptive Ion-Kinetic Electron-Fluid hybrid simulation model

(AIKEF) [*Müller et al.*, 2011] to the near-Callisto environment, which treats ions as particles and electrons as a massless, charge-neutralizing fluid. *Liuzzo et al.* [2015] used a hybrid model at Callisto to study the interaction of the Jovian magnetospheric plasma with the moon's ionosphere. That work also investigated the magnetospheric interaction with the moon's induced dipole in isolation, similar to the study of *Lindkvist et al.* [2015]. A detailed description of the AIKEF hybrid model is given in the *Liuzzo et al.* [2015] study and references therein, so only a brief overview of the model's features is presented here.

In the AIKEF model, Callisto's atmosphere is represented by the two dominant neutral species at the moon, namely CO_2 and O_2. The model atmosphere is asymmetric between Callisto's ramside and wakeside hemispheres (see section 2.3 and especially equation (13) in *Liuzzo et al.* [2015] for further discussion). The representation of the atmosphere (surface number density, scale heights, and hemispherical asymmetry) is quantitatively consistent with all available observations and modeling studies in the literature, including those presented by *Carlson* [1999], *Kliore et al.* [2002], *Liang et al.* [2005], *Cunningham et al.* [2015], and *Vorburger et al.* [2015]. The column density of O_2 substantially dominates that of CO_2 by more than 2 orders of magnitude and greatly exceeds the abundances of any other trace gases (e.g., H_2O, CO, O, or H) predicted by models of Callisto's atmosphere [cf. *Liang et al.*, 2005; *Vorburger et al.*, 2015]. Therefore, after ionization, individual trace gas species would merely act as test particles injected into a predefined electromagnetic field configuration and would not make any measurable contributions to the magnetic signatures near the moon. Since this study focuses on Callisto's electromagnetic environment, these trace species are not included in the atmosphere model of our hybrid code.

Callisto's ionosphere is generated from its neutral atmosphere through a combination of photoionization and electron impact ionization, using the wavelength-dependent EUVAC (solar EUV flux model for aeronomic calculations) photoionization model [*Richards et al.*, 1994] and isotropic precipitation of energetic electrons onto Callisto's atmosphere. Unlike the ionospheres of the other three Galilean moons, Callisto's ionosphere is mainly generated by photoionization [see *Seufert*, 2012; *Liuzzo et al.*, 2015]. For further details on the ionosphere model, the reader is referred to section 2.4 of *Liuzzo et al.* [2015]. Our preceding study also demonstrated that the fine structure of Callisto's atmosphere and the moon's orbital position (defined by its local time) have only minor quantitative impacts on the magnetic field near the moon.

The magnetic dipole induced in Callisto's subsurface ocean is incorporated by the method presented in *Kivelson et al.* [1999] and *Zimmer et al.* [2000]: the vastly different timescales of the plasma interaction and induction effects (minutes compared to hours, respectively) suggest that the induced field during a specific flyby can be represented by a constant dipolar magnetic moment [*Neubauer*, 1999; *Seufert et al.*, 2011]. Therefore, the induced field in our C10 simulations is represented by a static dipole located at the center of Callisto. Treating the subsurface ocean as a highly conducting medium whose induced currents generate a secondary magnetic field exactly canceling the primary field at the "magnetic poles" of the moon, the induced magnetic moment is represented as

$$\mathbf{M}_{\text{ind}} = -\frac{2\pi R_C^3}{\mu_0} \left(B_{x,0}\hat{\mathbf{x}} + B_{y,0}\hat{\mathbf{y}} \right) , \tag{1}$$

where $B_{x,0}$ and $B_{y,0}$ are the components of the magnetospheric background field vector $\mathbf{B}_0 = \left[B_{x,0}\hat{\mathbf{x}} + B_{y,0}\hat{\mathbf{y}} + B_{z,0}\hat{\mathbf{z}} \right]$ (see *Kivelson et al.* [1999] and *Zimmer et al.* [2000] for further details). This representation of the induced field is similar to the approach of, for example, *Liuzzo et al.* [2015] and *Lindkvist et al.* [2015] for Callisto and *Rubin et al.* [2015] for Europa.

Throughout the course of the C10 flyby, the observed background magnetic field $\mathbf{B}_0$ was slightly inhomogeneous, as visible in Figure 4c of *Kivelson et al.* [1999] (see also Figures 3 and 5 in this study and discussion in section 4). Comparing the inbound and outbound values measured by the spacecraft, the $B_{y,0}$ component of the background magnetic field shows the strongest variation. During $\pm$ 30min around C/A (corresponding to a distance traveled by the spacecraft of approximately 12 R_C in the $\hat{\mathbf{y}}$ direction), the $B_{y,0}$ component increased by nearly 14 nT. To represent this gradient in the model, we include a spatially inhomogeneous background magnetic field vector throughout the simulation domain. To fulfill $\nabla \cdot \mathbf{B}_0 = 0$, the field must also be weakly inhomogeneous in the $\hat{\mathbf{z}}$ direction. The background magnetic field vector is therefore set to

$$\mathbf{B}_0 = \left[0.00\hat{\mathbf{x}} + \left(\frac{y}{R_C} + 28.74 \right) \hat{\mathbf{y}} - \left(\frac{z}{R_C} + 11.00 \right) \hat{\mathbf{z}} \right] \text{nT} . \tag{2}$$

To calculate $B_{x,0}$ and $B_{y,0}$ needed for equation (1), we averaged $\mathbf{B}_0$ over the 10min interval between 00:39:37 and 00:49:37 on 17 September 1997. This interval directly follows the region around closest approach where the magnetospheric background field was completely obscured by Callisto's plasma interaction. This corresponds to an induced dipole magnetic moment at Callisto of

$$\mathbf{M}_{\text{ind}} = \left[M_x \hat{\mathbf{x}} + M_y \hat{\mathbf{y}}\right] = \left[0.00\hat{\mathbf{x}} - 2.42 \cdot 10^{18}\hat{\mathbf{y}}\right] \text{Am}^2. \qquad (3)$$

The value of $|\mathbf{M}_{\text{ind}}|$ here is nearly identical to the induced magnetic moment calculated by *Zimmer et al.* [2000] for the C3 ($|\mathbf{M}_{\text{ind}}| = 2.22 \cdot 10^{18}$ Am^2) and C9 ($|\mathbf{M}_{\text{ind}}| = 2.36 \cdot 10^{18}$ Am^2) flybys, which is consistent with Callisto being approximately at the same distance from the center of Jupiter's current sheet during these three encounters.

Over 80 simulations for the C10 flyby have been performed, using different upstream plasma parameters and orientations of the incident flow velocity vector $\mathbf{u}_0$. Two of the most insightful runs are presented in this study. Because the upstream conditions at Callisto are not well constrained at the time of the flyby, the simulations use average plasma parameters for the moon's orbital distance, obtained from *Kivelson et al.* [2004]. For the runs presented here, the upstream magnetospheric plasma is assumed to consist of singly charged 16 amu oxygen ions with a number density of 0.35 cm^{-3} and a temperature of 100 eV. An ambient flow speed of $u_0 = 271.5$ km/s relative to Callisto is used, corresponding to 83% of magnetospheric corotation at the orbit of the moon, consistent with the recent results of *Bagenal et al.* [2016]. These values amount to a sub-Alfvénic and submagnetosonic upstream plasma, with an Alfvénic Mach number of $M_A = 0.808$ and a magnetosonic Mach number of $M_{\text{MS}} = 0.802$. Each of the values used here is within its respective range suggested by *Kivelson et al.* [2004] for the orbital distance of Callisto. In this configuration, the upstream ions as well as the ionospheric O_2^+ and CO_2^+ species possess gyroradii r_g comparable to the size of the moon, with $r_{g,O^+} = 0.52\,R_C$, $r_{g,O_2^+} = 1.03\,R_C$, and $r_{g,CO_2^+} = 1.42\,R_C$. The large gyroradii thereby confirm the necessity of a kinetic representation of the ions near Callisto.

For both simulations, a simulation domain of $-8\,R_C \leq x \leq 8\,R_C$ and $-10\,R_C \leq y, z \leq 10\,R_C$ with two levels of static mesh refinement is used. A maximum grid resolution of 49 km/cell is achieved within the moon's ionosphere. The first run presented in sections 4.1 and 4.2 assumes purely azimuthal magnetospheric flow; i.e., $\mathbf{u}_0 = u_0\hat{\mathbf{x}}$. The second run presented in section 4.3, however, assumes a deviation from corotation by $\phi = 20°$ into the Jupiter-facing ($y > 0$) hemisphere; i.e., $\mathbf{u}_0 = u_0\left[\cos(\phi)\hat{\mathbf{x}} + \sin(\phi)\hat{\mathbf{y}}\right]$.

4. Model Results, Data Analysis, and Discussion

4.1. Callisto's Plasma Interaction During the C10 Flyby

The global structure of Callisto's magnetic and plasma environment during the C10 flyby is depicted in Figure 2 for the simulation with its upstream velocity $\mathbf{u}_0$ aligned with the direction of corotation. Figure 2a displays the three-dimensional structure of the draped magnetic field near Callisto from a vantage point downstream of the moon ($x > 0$) and in its Jupiter-facing ($y > 0$) hemisphere. The trajectory of the C10 flyby is displayed in black, with the spacecraft's direction of travel indicated by bold arrows. Illustrated at the edges of the simulation domain are vectors of the magnetospheric background field $\mathbf{B}_0$, with the faces color coded to the field magnitude $|\mathbf{B}_0|$. Light blue regions correspond to larger values of $|\mathbf{B}_0|$, whereas light yellow regions correspond to lower values. Clearly visible is the slight inhomogeneity of the background field, especially in the $\hat{\mathbf{y}}$ direction.

The draped field lines of the Alfvén wings are visible near the moon, inclined at an angle of approximately 40° against the background field (Figure 2a). As the upstream plasma is decelerated due to mass loading in Callisto's ionosphere, the frozen-in magnetospheric field lines pile up at the ramside of the moon but continue to convect toward downstream at its flanks, thereby generating the tilted Alfvén wing characteristics. No bow shock is formed upstream of Callisto. In Figure 2a, the Alfvén wings are color coded to illustrate regions of (red) positive and (blue) negative B_x (i.e., the field component along the direction of corotation). As the local magnetospheric background field $\mathbf{B}_0$ is nearly aligned with the $+y$ axis, the Alfvén wings are mainly confined to Callisto's equatorial ($z = 0$) plane in the immediate vicinity of the moon. When moving along the magnetospheric field lines toward Jupiter and farther from Callisto, the Jovian magnetic field becomes more dipolar and the Jupiter-facing Alfvén wing ($y > 0, B_x > 0$) connects to Jupiter's south polar ionosphere, whereas the Jupiter-averted wing ($y < 0, B_x < 0$) connects to the giant planet's north polar ionosphere. However, these effects would take place outside the boundaries of our simulation domain.
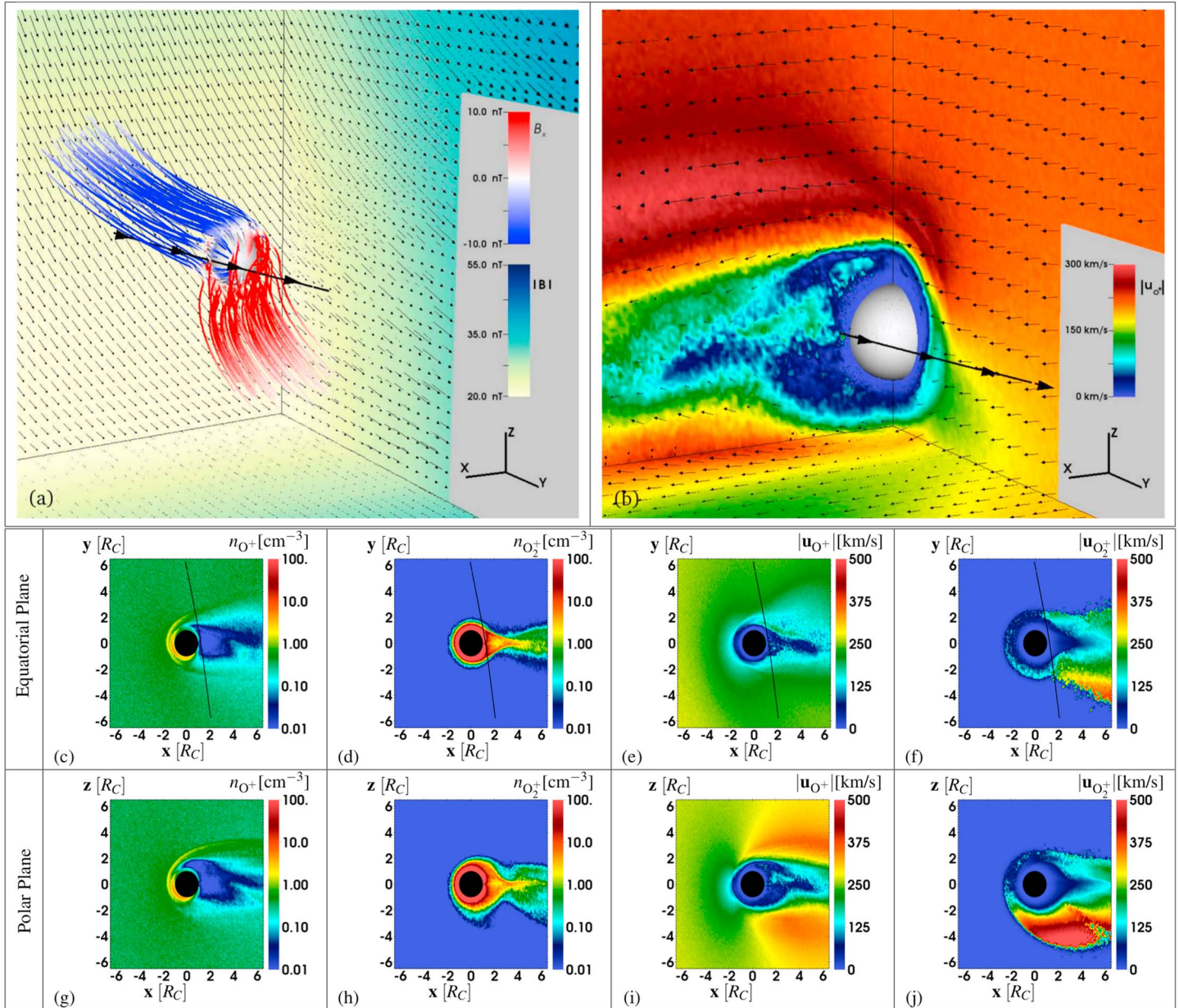
Figure 2. The global structure of Callisto's magnetic and plasma environments during the C10 encounter. (top row) (a) Three-dimensional structure of the magnetic field **B** near Callisto in the simulation domain. Magnetic field lines near the moon are color coded, corresponding to (red) positive and (blue) negative perturbations of B_x. The faces of the simulation ($x = -8\,R_C$, $y = -10\,R_C$, $z = -10\,R_C$) are colored according to the magnitude of the slightly inhomogeneous *background* magnetospheric field $|\mathbf{B}_0|$ and include vectors of $\mathbf{B}_0$. The trajectory and direction of the C10 flyby is included in black. (b) Three-dimensional structure of the magnetospheric plasma velocity $\mathbf{u}_{O^+}$ in the $x = 0\,R_C$, $y = 0\,R_C$, and $z = -2\,R_C$ planes. Orange represents the background flow velocity $|\mathbf{u}_0|$, red hues represent $|\mathbf{u}_{O^+}| > |\mathbf{u}_0|$, and green/blue hues represent $|\mathbf{u}_{O^+}| < |\mathbf{u}_0|$. Flow vectors of $\mathbf{u}_{O^+}$ are shown for the three cutting planes, and the C10 trajectory is included. The vantage point for Figures 2a and 2b is located downstream of Callisto ($x > 0$) and in its Jupiter-facing ($y > 0$) hemisphere. (middle row) Plasma parameters in Callisto's equatorial ($z = 0$) plane. The number densities of (c) magnetospheric O^+ ions and (d) ionospheric O_2^+ ions are displayed, along with the projection of the C10 flyby trajectory. The background number density ($n_0 = 0.35$ cm^{-3}) is indicated in green, with increases above background represented by red hues, and reductions below background represented by blue hues. Bulk velocities of (e) magnetospheric O^+ ions and (f) ionospheric O_2^+ ions are also displayed. The background bulk velocity ($|\mathbf{u}_0| = 271.5$ km/s) is indicated in yellow. Bulk velocities larger or smaller than $|\mathbf{u}_0|$ are in red or blue hues, respectively. (bottom row) Plasma parameters in Callisto's polar ($y = 0$) plane. The number density of (g) magnetospheric O^+ and (h) ionospheric O_2^+ ions, along with the bulk velocity of the (i) magnetospheric and (j) ionospheric ions, are included. Colors are as in Figures 2c–2f. Please note that the x axis in Figures 2a and 2b points in the opposite direction compared to that in Figures 2c–2j.

Figure 2b displays the bulk velocity of magnetospheric O^+ ions near Callisto in the $x = 0\,R_C$, $y = 0\,R_C$, and $z = -2\,R_C$ planes from the same vantage point as Figure 2a. The undisturbed, upstream bulk velocity $|\mathbf{u}_0|$ is illustrated in orange, with vectors of the flow velocity included. The magnetospheric plasma is accelerated above and below the moon to approximately 1.5 times the magnetospheric background velocity as it is diverted around Callisto's ionosphere and induced dipole. In the moon's immediate vicinity, mass loading causes nearly complete stagnation of the upstream plasma to less than 1% of $|\mathbf{u}_0|$. This is consistent with analytical estimations of the flow speed near Callisto [*Strobel et al.*, 2002]. The region of reduced O^+ flow speed is clearly visible downstream and extends more than $6\,R_C$ along the $+x$ axis. At these distances, the magnetospheric plasma is redirected into the wake. This is visible in the vectors of the flow velocity that are directed toward Callisto's geometric shadow downstream of the moon.

Two-dimensional cuts through Callisto's interaction region are presented in Figures 2c–2j. Figures 2c and 2d show the number density, and Figures 2e and 2f the bulk velocity of the upstream O^+ ions and ionospheric O_2^+ ions, respectively, in the $z = 0$ plane. The C10 flyby took place nearly in this plane (with $z \approx -0.09\,R_C$ during the encounter), and a projection of the trajectory onto the $z = 0$ plane is included. Figures 2c and 2e show a cavity in the magnetospheric density and a reduced velocity of the magnetospheric ions downstream of Callisto (also visible in Figure 2b), as the upstream plasma is diverted around the moon. The wakeside number density of the ionospheric plasma, however (see Figure 2d), exceeds the upstream number density $n_0 = 0.35\,\text{cm}^{-3}$ by nearly 3 orders of magnitude as the freshly produced ions are picked up by the magnetic field and convected toward downstream. Because the large cycloidal arcs associated with pickup ion motion are mainly located in the polar ($y = 0$) plane, the slowly moving cold plasma in the equatorial plane is essentially confined to the narrow region of Callisto's geometric shadow. While only few ionospheric particles exit this region due to the slight component of $\mathbf{B}_0$ along $-\hat{\mathbf{z}}$, these particles are accelerated to velocities above $|\mathbf{u}_0| = 271.5\,\text{km/s}$ in the $y < 0$ hemisphere of Callisto (see Figure 2f).

Also visible in Figure 2d is the formation of a split tail structure of the escaping O_2^+ ions beyond $x = 1.5\,R_C$ downstream, with two distinct filaments of slightly increased ionospheric density (depicted in dark red) and a region of lower density in between (depicted in yellow). These filaments subsequently merge into a single tail near $x \approx 4\,R_C$. Similar filamented tail signatures of escaping ionospheric particles have been observed during the T9, T63, and T75 Cassini flybys of Saturn's largest moon Titan [*Coates et al.*, 2012], whose ambient plasma environment (e.g., Alfvénic Mach number, pickup ion gyroradii, and magnetospheric background field strength) is very similar to that of Callisto [*Simon et al.*, 2015]. These filamented tail structures were determined to be an omnipresent characteristic of Titan's pickup tail region, with detection or nondetection highly dependent on the Cassini flyby trajectory [*Feyerabend et al.*, 2015].

Figure 2d shows that the C10 encounter occurred too close to Callisto, with the split tail developing too far downstream, to allow for detection of filamentation in the moon's tail (see also further discussion of the electron density measurements in section 4.2.4). Figure 2d also suggests that for Callisto flybys farther from the moon, filamented channels of increased ion density may be observable. For instance, the C22 flyby on 14 August 1999 with a C/A altitude of nearly $1\,R_C$ may have been a good candidate to observe the split tail structure at Callisto. Similar to the C10 encounter, the C22 trajectory was located at the wakeside and near Callisto's equatorial plane, but C/A occurred more than 4 times farther from the moon. Although time series of the plasma moments have not been published for the C22 flyby, *Gurnett et al.* [2000] used data from the Galileo plasma wave instrument to identify a narrow region of abrupt electron density enhancement just outside of Callisto's geometric shadow. This observed feature may be explained by enhanced ionospheric outflow along one of the density filaments in the moon's wake. The orientation of the C22 trajectory would have been suitable to detect these structures.

Particle gyration occurs mainly in the polar ($y = 0$) plane of Callisto's interaction, shown in Figures 2g–2j, which is nearly perpendicular to $\mathbf{B}_0$. The Galileo C10 trajectory intersected this plane at only a single point downstream of the moon. In the polar plane, the deflection and acceleration of the magnetospheric plasma at the flanks of Callisto are both slightly asymmetric between the moon's northern ($z > 0$) and southern ($z < 0$) hemispheres, visible in Figures 2g and 2i. Outside of Callisto's geometric shadow, the magnetospheric plasma reaches peak velocities up to approximately $1.4|\mathbf{u}_0|$, whereas the magnetospheric bulk velocity is reduced to below 1 km/s within the shadow.

The model results for the $y = 0$ plane also show that the density and velocity structures of ionospheric O_2^+ are asymmetric between the moon's northern and southern hemispheres (see Figures 2h and 2j). As ionospheric
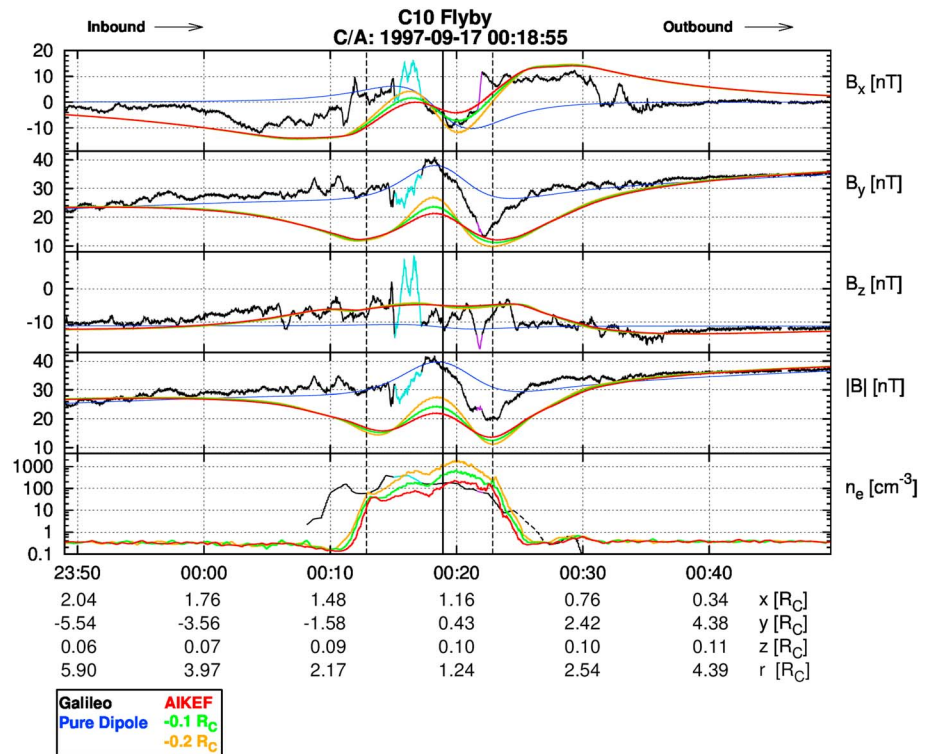
Figure 3. Galileo observations and modeled results for the C10 flyby. (first to fifth panels) B_x, B_y, and B_z components of the magnetic field, the magnitude of the field $|\mathbf{B}|$, and the electron number density n_e. Black vertical lines correspond to the location of (dashed) Callisto's geometric shadow and (solid) closest approach of Galileo at 00:18:55. The spacecraft position (x, y, z, and $r = \sqrt{x^2 + y^2 + z^2}$ in CphiO coordinates) along the flyby trajectory is included below the fifth panel. In black are the magnetic field and electron density data measured by the spacecraft. The (turquoise) M-like feature and the (purple) rotational discontinuity detected by Galileo are discussed in the text. Blue lines represent the pure dipole approximation calculated from equation (1). The dipole approximation does not consider any plasma perturbations, so there is no blue line in the electron density panel. For the hybrid simulation with upstream flow $\mathbf{u}_0$ aligned with $\hat{\mathbf{x}}$, results along the C10 trajectory are included in red, while results along trajectories shifted by 0.1 R_C and 0.2 R_C toward Callisto along the $-\hat{\mathbf{x}}$ direction are displayed in green and orange, respectively.

particles are picked up and convected downstream, they experience the ambient electromagnetic fields and gyrate into the $z < 0$ hemisphere on cycloidal trajectories. As described by *Liuzzo et al.* [2015], the pickup ion population causing the asymmetries in the velocity field outside of Callisto's geometric shadow is too dilute to generate a noticeable density enhancement (Figure 2h), but these particles are accelerated to approximately $2|\mathbf{u}_0|$ along their cycloidal arcs (Figure 2j).

4.2. Comparison to Data From the C10 Flyby
4.2.1. Alfvén Wing and Dipole Signatures in B_x

Magnetic field components and electron number density from the hybrid model run with $\mathbf{u}_0$ along $\hat{\mathbf{x}}$ are compared to observations by the Galileo spacecraft in Figure 3. The dashed vertical lines near 00:13 and 00:23 represent Galileo's inbound and outbound passages through the surface of Callisto's geometric shadow (defined by $\sqrt{y^2 + z^2} \leq R_C$ and $x > 0$), and the solid vertical line near 00:19 marks the time of closest approach (C/A) to the moon. Plotted in black are magnetic field and electron density data recorded during the flyby. As can be seen, equation (2) provides an accurate representation of the slight inhomogeneity in the magnetospheric background field $\mathbf{B}_0$ near Callisto.

The blue lines in Figure 3 illustrate the magnetic signatures generated along the C10 trajectory by a pure dipole field induced in the moon's interior. The dipolar magnetic moment has been calculated using equation (1) and therefore does not consider the plasma interaction currents from the hybrid code. This setup only represents a first approximation to Callisto's magnetic environment. We present results for the pure dipole here as this approach was successfully applied by *Khurana et al.* [1998], *Kivelson et al.* [1999], and *Zimmer et al.* [2000] to explain magnetic field perturbations observed during the C3 and C9 flybys. The red lines in

Figure 3 are based on a more accurate representation of Callisto's magnetic and plasma environment using the AIKEF hybrid model. Given the uncertainties in the upstream and atmosphere parameters during C10, the locations, magnitudes, and extensions of the modeled plasma and magnetic signatures are associated with some degree of uncertainty. Therefore, data along two "virtual" trajectories shifted closer to Callisto are also included in the figure, with green and orange lines representing shifts of 0.1 R_C and 0.2 R_C in the $-\hat{\mathbf{x}}$ direction, respectively.

Along the inbound segment of the flyby, the Galileo spacecraft measured a negative perturbation in the B_x component (δB_x) beginning around 00:00 and ending near 00:10. This perturbed region extended more than 2 R_C into the Jupiter-averted hemisphere of Callisto, and B_x remained depressed to approximately -10 nT throughout most of the feature. Superimposed were short-scale magnetic field fluctuations, probably associated with the north-south motion of Jupiter's magnetospheric current sheet. These field variations had a magnitude of approximately 1 nT and were most likely unrelated to Callisto's local plasma interaction. The first $\delta B_x < 0$ segment of the flyby trajectory was then succeeded by a region where B_x increased up to $+15$ nT as the spacecraft entered Callisto's geometric shadow. This enhancement was again followed by a negative δB_x signature, where B_x was reduced to values near ≈ -10 nT after C/A. As the spacecraft exited the moon's geometric shadow, a second plateau-like perturbation in B_x was detected and increased to a nearly constant value of $+10$ nT for more than 2 R_C along the y axis. Galileo left this plateau-like region around 00:31, after which the perturbed B_x component returned to its background value of $B_{x,0} \approx 0$. We will demonstrate that this sequence of four alternating B_x perturbations was a result of the coupling between the moon's plasma interaction and induction within its subsurface ocean.

As is visible in the blue curve in Figure 3, a pure dipole magnetic field agrees well with spacecraft observations of B_x in the central region of Callisto's geometric shadow. However, closer to the edges of the shadow, the measured B_x component deviates from the pure dipole approximation: while the dipole returns to the background value of $B_{x,0} \approx 0$, the observed B_x component displays sharp transitions to the two plateau-like features inbound and outbound of Callisto's geometric shadow. The poor agreement between a pure dipole and the data is expected at larger distances to Callisto, as the plasma interaction during this flyby was much stronger than during C3 and C9 [*Zimmer et al.*, 2000].

When induction within Callisto's subsurface ocean and the plasma interaction are both considered (depicted by the red, green, and orange lines in Figure 3), the modeled B_x agrees much better with observations. For the C10 trajectory and the two shifted trajectories, the two regions of alternating B_x within the moon's geometric shadow are still qualitatively reproduced and are now slightly deformed compared to the pure dipole case (blue). The modeled bipolar B_x perturbations along the shifted trajectories are slightly more pronounced than the modeled B_x perturbations along the actual flyby trajectory in this region. Particularly within the shadow, trajectories shifted closer to the moon display a stronger dipole signal than the actual C10 trajectory, but qualitatively similar signatures can be seen along each curve. Thus, the observed and modeled B_x signatures within the geometric shadow are fairly robust against slight changes in the trajectory.

As visible in Figure 3, the hybrid model also succeeds in reproducing the two regions of enhanced $|B_x|$ in the inbound and outbound segments of the flyby. Outside of Callisto's geometric shadow, the modeled magnitude of the B_x perturbations agrees with Galileo data reasonably well. This improvement in the modeled results compared to the pure dipole approximation shows that including the plasma interaction is paramount in understanding the C10 observations.

To reveal the origin of the observed B_x reversals, Figure 4 illustrates the modeled components of the magnetic field near the moon in its equatorial ($z=0$) plane. Draping of the magnetospheric background field gives rise to Alfvén wing characteristics which intersect the C10 trajectory twice and extend to large distances from Callisto. These wings are clearly visible in Figure 4b, which depicts the B_x component of the magnetic field from the hybrid simulation. In analogy to Figure 2a, the wing with (red) positive B_x is located in Callisto's Jupiter-facing ($y>0$) hemisphere, while the wing with (blue) negative B_x is located in the moon's Jupiter-averted ($y<0$) hemisphere. Directly downstream of Callisto, however, the B_x orientation is reversed with (blue) negative B_x in the $y>0$ hemisphere and (red) positive B_x in the $y<0$ hemisphere. This reversal in B_x close to the moon corresponds to the magnetic signature of Callisto's induced dipole field. Hence, this quasi-dipolar "core region" of the interaction directly downstream of Callisto is partially shielded from the magnetospheric plasma interaction with the moon [see also *Liuzzo et al.*, 2015] and still displays a nearly unobscured
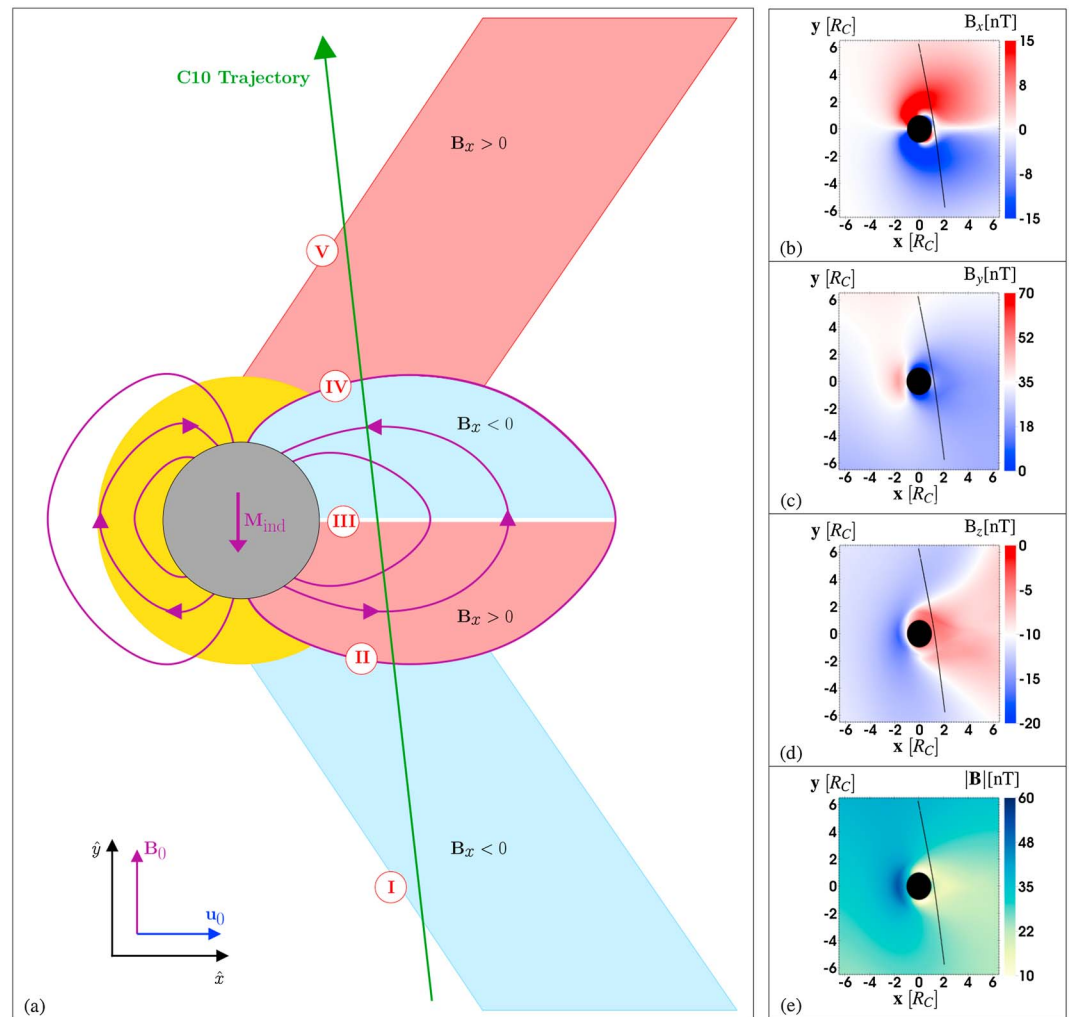
Figure 4. (a) Schematic illustration of the magnetic field near Callisto in the moon's equatorial ($z=0$) plane. Callisto's ionosphere is represented in yellow, and its induced magnetic moment and resulting quasi-dipolar field lines are in magenta. Also included in green is the projection of the Galileo C10 flyby onto this plane. Red and blue hues correspond to regions of positive and negative δB_x. In the vicinity of Callisto, the magnetic environment is dominated by the quasi-dipolar induced field, whereas at larger distances, the field perturbations are generated by the moon's Alfvén wings. Numerals I–V denote transitions between regions with different orientations of B_x and are discussed in the text. Modeled (b) B_x, (c) B_y, and (d) B_z components of the magnetic field in the $z=0$ plane, with the projection of the C10 trajectory included in black. The background values of each component are in white, whereas positive and negative perturbations are in red and blue, respectively. (e) Magnetic field magnitude, $|\mathbf{B}|$, in the $z=0$ plane. The background values of $|\mathbf{B}_0|$ are indicated by light blue, and dark blue hues represent an increase in $|\mathbf{B}|$, whereas light yellow hues represent a decrease in $|\mathbf{B}|$. Please note that the schematic in Figure 4a *is not* to scale, as the region dominated by the dipole has been drastically enlarged to better highlight transitions between the different field regimes. As visible in Figure 4b, the induced dipolar field is actually confined to a small region near Callisto's wakeside surface (due to the strong r^{-3} decrease of the dipole field with distance).

induction signal. Thus, in this region it should be possible to identify the induction signature of Callisto's subsurface ocean during close wakeside encounters, even when the moon's plasma interaction is strong.

Magnetic features in the near-Callisto environment are therefore generated by two competing effects. On the one hand, induction within the subsurface ocean generates a quasi-dipolar magnetic field that is nearly unobscured close to the moon and in its wake. On the other hand, the plasma interaction and draping generate Alfvén wings farther away from Callisto. The Galileo spacecraft detected both of these regimes during the C10 encounter. Figure 4a displays a schematic illustration of the B_x component (again with $B_x>0$ in red and $B_x<0$ in blue) in the equatorial plane near Callisto during C10. During Galileo's approach toward Callisto, the spacecraft first intersected the region of negative B_x, corresponding to the moon's Jupiter-averted ($y<0$)

Alfvén wing, which eventually connects to the giant planet's north polar ionosphere. This occurred between approximately 00:00 and 00:10 in Figure 3 and between the points marked I and II in Figure 4a. The spacecraft then detected the $y < 0$ hemisphere of the induced dipole (between points II and III) where the field lines point away from Callisto ($B_x > 0$), visible in the observed B_x component between 00:10 and 00:16.

Galileo continued to move through Callisto's geometric shadow and crossed the $y = 0$ plane directly downstream of the moon and at $x \approx 1.2\,R_C$. Here B_x changed its sign as the dipole field lines were locally aligned with the $+y$ axis. This is visible in Figure 3 at 00:17 just prior to closest approach where $B_x \approx 0$. The fact that this B_x polarity reversal was detected by Galileo at $y \approx 0$ confirms that Callisto's induced magnetic moment was indeed aligned with the $-y$ axis during this flyby and is therefore accurately represented in the model setup. After Galileo crossed this layer of $B_x \approx 0$, it entered the moon's Jupiter-facing hemisphere where the field lines of the induced dipole return to Callisto and were therefore oriented along $-\hat{\mathbf{x}}$. This hemisphere of the dipole was crossed between points III and IV in Figure 4a, also visible in the observed B_x between 00:17 and 00:21 (Figure 3). Following this region, Galileo exited the dipole-dominated region near 00:22 and entered the moon's Jupiter-facing Alfvén wing (which eventually connects to the planet's south polar ionosphere), characterized by a positive B_x component. This occurred between points IV and V in Figure 4a. Finally, after approximately 00:31, the Galileo spacecraft exited the Jupiter-facing Alfvén wing (point V in Figure 4a), and B_x returned to its background value of $B_{x,0} \approx 0$ nT.

Despite the overall agreement between the modeled and observed Alfvén wing structures in B_x, discrepancies manifest in the *sharpness* of the transitions to the undisturbed background magnetic field in the inbound and outbound regions of the flyby. While the model suggests a gradual transition from $B_{x,0} \approx 0$ nT to the plateau-like B_x perturbations, the observed B_x signature displayed rather sharp changes at the outer edges of the wings (around 00:00 and 00:31 in Figure 3). This was especially evident near the outbound crossing of the Jupiter-facing wing at 00:31 (marked by point V in Figure 4a) where the draped field returned to its background value of $B_{x,0} \approx 0$ nT over a scale of only $0.15\,R_C$ in the $\hat{\mathbf{y}}$ direction.

To explore possible origins of these discrepancies, the hybrid model was run with reduced atmospheric scale heights, neutral gas densities, and ionization rates. However, doing so not only diminished the extension of the Alfvénic B_x perturbations but also decreased their magnitude way below the observed values. Given the vast uncertainties in the upstream and obstacle parameters during C10, further investigation of the *sharpness* of the B_x features near the outer edges of the wings is reserved for future work.

The observed magnetic field also displayed a steep jump at the interface of the dipole and the Jupiter-facing Alfvén wing between 00:21:36 and 00:22:02 in Figure 3, corresponding to point IV in Figure 4a. This segment of the magnetic field and plasma data is highlighted in purple in all panels of Figure 3. The sharpness of this feature was especially visible in the B_x component which changed from -4 nT to $+12$ nT on a length scale of only $0.09\,R_C$ in the $\hat{\mathbf{y}}$ direction. It is also visible in B_y which jumped from 18 nT to 14 nT. Simultaneously, B_z displayed a spiked structure, but the values of B_z at the start (00:21:36) and end (00:22:02) of the magnetic field jump were nearly identical ($B_z \approx -13$ nT). During this time frame, $|\mathbf{B}|$ remained nearly constant. Therefore, throughout this region, the magnetic field vector ($B_x \hat{\mathbf{x}} + B_y \hat{\mathbf{y}}$) in the $z = 0$ plane rotated by an angle of 53° in the clockwise direction (i.e., toward downstream).

To characterize this jump, we performed a minimum variance analysis [*Sonnerup and Cahill*, 1967] of the magnetic field data between 00:21:36 and 00:22:02. The three eigenvalues (λ_{min}, λ_{med}, and λ_{max}) of the variance matrix read $\lambda_{min} = 0.1439$, $\lambda_{med} = 1.7326$, and $\lambda_{max} = 29.4151$, yielding a ratio of $\frac{\lambda_{min}}{\lambda_{med}} = 0.083$ between the smallest and intermediate eigenvalues. This small ratio indicates that the observed field jump was indeed a discontinuity, whose normal vector (corresponding to λ_{min}) was $\mathbf{e}_{min} = [0.2206\hat{\mathbf{x}} + 0.9396\hat{\mathbf{y}} - 0.2616\hat{\mathbf{z}}]$. The vector $\mathbf{e}_{min}$ pointed mainly in the $\hat{\mathbf{y}}$ direction, and as a result, the discontinuity was nearly perpendicular to the slightly stretched dipole field lines in Callisto's geometric shadow. Given the constancy of $|\mathbf{B}|$, it is therefore highly likely that Galileo crossed a *rotational discontinuity* when leaving the core region of the quasi-dipolar field and entering Callisto's Jupiter-facing Alfvén wing. At this discontinuity, the magnetic field rotated from pointing toward the moon ($B_x < 0$ in the quasi-dipolar field) to pointing away from the moon ($B_x > 0$ in the Jupiter-facing Alfvén wing). The interpretation of this magnetic field jump as a rotational discontinuity is further supported by the constancy of the measured electron density during this time period, visible in Figure 3. Since the extension of this discontinuity was less than $0.1\,R_C$ along $\hat{\mathbf{y}}$, it would be confined to only a few cells in the simulation. Therefore, this structure would be extremely difficult to resolve in the hybrid model whose magnetic field output is also subject to a small amount of numerical diffusion [see also *Kriegel et al.*, 2014].

This clear demarcation between the dipole-dominated region and Alfvén wing dominated region downstream of Callisto may prove useful for the disentanglement of induction and plasma interaction signatures in magnetic field data from future flybys. It is important to note that at Callisto's ramside, however, the induced dipole is completely obscured by the signatures of pileup and draping of the magnetospheric field around the moon's ionosphere. Thus, there is no quasi-dipolar core region in Callisto's ramside hemisphere that would permit an easy identification of the induction signal from the subsurface ocean.

4.2.2. Draping and Dipole Signatures in B_y

As is visible in Figure 3, the measured B_y component was nearly featureless during the inbound portion of the C10 encounter, except for short-scale magnetospheric fluctuations and the slight inhomogeneity of the background field. After entering Callisto's geometric shadow near 00:13, the spacecraft detected a bipolar perturbation, consisting of an increase to a peak value of $B_y = 40$ nT around 00:17, followed by a drop to a value of $B_y = 15$ nT near 00:21. Just prior to exiting Callisto's geometric shadow, B_y began to return to the background value of $B_{y,0} \approx 31$ nT.

The pure dipole approximation plotted in blue in Figure 3 agrees reasonably well with the observed B_y during the inbound segment of the flyby until 00:20, which corresponds to a spacecraft position deep within the moon's geometric shadow. Hence, the quasi-dipolar core region of Callisto's wake that was identified in the B_x component is also visible in B_y (corresponding to the B_y enhancement near 00:17). However, the second half of the bipolar perturbation that was observed between 00:20 and 00:25 is not replicated by the pure dipole model.

Although the dipole alone is able to explain the enhancement observed in B_y near C/A, the modeled feature is slightly too broad. The width is more accurately represented when Callisto's plasma interaction is considered. This is visible in the red, green, and orange lines in Figure 3, although the magnitude of the peak at 00:17 is clearly not reached. However, the minimum value of B_y that occurred near 00:22 is reproduced very well by the hybrid model for all three trajectories (one real and two shifted), and its location is also in reasonable agreement with the observation. The modeled width of this decrease is larger than the observed width of the feature but is consistent with the hybrid model results for B_x in the outbound segment of the trajectory.

This outbound depression in B_y corresponds to Callisto's Jupiter-facing Alfvén wing, also visible in B_x in the same region. As shown in Figures 3 and 4b, draping of the magnetospheric background field around Callisto caused an increase in $|B_x|$ during the inbound and outbound segments of the flyby (as discussed in section 4.2.1). Simultaneously, the "kink" in the field lines due to draping causes the modeled B_y to decrease on both sides of the moon. This signature is visible in the modeled B_y component between 00:00–00:12 and 00:22–00:30 (see Figure 3) and also in the equatorial, two-dimensional cut of B_y illustrated in Figure 4c. However, despite the strong draping signature in B_x, the measured B_y along the inbound portion of the trajectory does not show any depression feature at all that would be indicative of magnetic field line draping.

As shown by *Liuzzo et al.* [2015], any asymmetries due to large ion gyroradii near Callisto should only manifest in planes perpendicular to $\mathbf{B}_0$, but not in the flyby plane which was approximately parallel to $\mathbf{B}_0$. Indeed, the observed draping signature in B_x was nearly symmetric with respect to the $y = 0$ line during C10, as expected from the geometry of the flyby and considering that $\mathbf{B}_0$ was mainly aligned with the y axis (i.e., the background field was perpendicular to $\mathbf{u}_0$). The draping signature in B_x was characterized by similar values of $\delta B_x \approx \pm 10$ nT outside of Callisto's geometric shadow (corresponding to the regions I–II and IV–V in Figure 4a). In the B_x data, the extension of the Jupiter-averted wing along the spacecraft trajectory (with a width of approximately 2.0 R_C) was slightly larger than that of the Jupiter-facing wing (with a width of approximately 1.6 R_C). This difference was likely caused by the 11.6° counterclockwise rotation of the flyby trajectory around the point of C/A (see Figures 1 and 4a). Therefore, this observed B_x draping pattern was nearly symmetric and should have been accompanied by a symmetric B_y counterpart.

The expected symmetry between the draping perturbations in B_x and B_y is accurately modeled by the hybrid simulation (see Figures 3, 4b, and 4c). At the ramside of Callisto, pileup of the magnetospheric field is visible in Figure 4c, whereas in the immediate vicinity of the moon's magnetic poles, B_y decreases below the background value of $B_{y,0}$. This decrease is mainly a result of the antialignment of $\mathbf{M}_{ind}$ and $\mathbf{B}_0$. At distances greater than 2 R_C, the induced field is weaker than 10% of the background field and is therefore negligible compared to $\mathbf{B}_0$. As a result, the modeled symmetric depressions of B_y farther from Callisto are primarily driven by the magnetospheric field line draping.

However, the expected symmetric B_y depletion was not observed during the C10 encounter. Although Galileo detected a B_y depression in Callisto's Jupiter-facing ($y > 0$) hemisphere which was associated with draping, the spacecraft did not observe a similar B_y depression in the Jupiter-averted ($y < 0$) hemisphere of the moon. Apart from the omnipresent magnetospheric fluctuations on the order of 1 nT, no significant deviation from the background field was observed in B_y until well inside of Callisto's geometric shadow, even in the region where the B_x measurements implied the location of the moon's Jupiter-averted Alfvén wing. Moreover, the B_y draping feature in the Jupiter-facing hemisphere was much narrower than its B_x counterpart; i.e., the plateau-like enhancement observed in B_x *does not* directly map into B_y.

The mechanism that generated this unexpected asymmetry in the observed B_y perturbations between the inbound and outbound segments of the trajectory is unknown but may have been magnetospheric in origin or may rather have arisen from a substantial local inhomogeneity in the density of Callisto's atmosphere at the time of C10. These suggestions cannot be substantiated, however, as the lack of suitable observations at the time of the encounter makes confirmation difficult. Regardless, the following is clear: in order to explain the measured B_y perturbations during the inbound segment of the C10 flyby, a pure dipole must be used. On the contrary, the measured B_y perturbations during the outbound segment of the encounter can only be explained when the moon's plasma interaction is considered.

In summary, the observed signatures of B_y are qualitatively consistent with a combination of plasma interaction and induction only beyond approximately 00:15, corresponding to the core region and outbound segment of the C10 trajectory. However, the complete absence of any perturbations in the observed B_y during the inbound segment is not only at odds with results from the hybrid model but is also inconsistent with the symmetric B_x draping signatures detected by Galileo.

4.2.3. B_z and Magnetic Field Strength

The observed and modeled B_z signatures are also presented in Figure 3. Galileo detected perturbations related to Callisto in this component starting near 00:00, where B_z began to display a plateau-like enhancement which lasted until 00:30. This plateau was characterized by perturbations of $\delta B_z \approx 5$ nT above the background value of $B_{z,0} \approx -11$ nT and extended for more than $6\,R_C$ along the C10 trajectory. However, features associated with Callisto's interaction are more difficult to identify in this component due to superimposed magnetospheric fluctuations on the order of $\delta B_z \approx 2$ nT. The B_z component also displayed a prominent M-like enhancement between 00:15 and 00:17 with an extension of $0.4\,R_C$ along the flyby trajectory, highlighted in turquoise in Figure 3. At the outer spikes of the M-like feature, B_z reached peak values of 9 nT, whereas B_z dropped to values of about -2 nT at the middle "valley" of the M feature. The M-like signature was the only region during the encounter where B_z reversed its sign for an extended time, from southward facing to northward facing. The M structure was also visible in B_x at the same time between 00:15 and 00:17. When entering this feature, Galileo detected a rotation of **B** around the y axis in a counterclockwise direction by approximately 100°.

The pure dipole model (blue line in Figure 3) shows only minimal B_z perturbations along the flyby trajectory, with the dipole field strength never deviating from $B_{z,0}$ by more than approximately 10%. The nearly vanishing δB_z perturbation of the dipole is expected, given the flyby geometry and the fact that $\mathbf{M}_{ind}$ is confined to the $z = 0$ plane.

The hybrid model, however, succeeds in reproducing the measured width and magnitude of the plateau in B_z. Near 00:05, the modeled B_z along all three trajectories (C10 in red and shifted in green and orange) increases from $B_{z,0} \approx -11$ nT to $B_z \approx -5$ nT. Around 00:24, the magnitude of the modeled B_z plateau region begins to gradually return to the background value of $B_{z,0}$. Hence, apart from the M-like feature, the model results are in good quantitative agreement with the observed structure of B_z. The plateau region is also visible in Figure 4d, which shows B_z in the equatorial ($z = 0$) plane of Callisto. The B_z component is slightly increased within the entire draping and Alfvén wing region downstream of Callisto. Considering the large Hall conductivity within Callisto's ionosphere [*Strobel et al.*, 2002], this region of enhanced B_z may be generated by the Hall effect which is mainly visible in the B_z component. The nonzero B_z maps into Callisto's Alfvén wings due to the translational symmetry of the wings along their characteristics [*Simon et al.*, 2011]. These nonzero B_z perturbations are also associated with the fact that the background field $\mathbf{B}_0$, which acts as a "guide" for the Alfvén waves, is slightly inclined with respect to the $z = 0$ plane.

Other than small-scale magnetospheric fluctuations which were likely unrelated to Callisto, the lone feature that the hybrid model does not reproduce is the narrow, M-like spike observed in B_z between 00:15 and 00:17.

This feature also mapped into the B_x component near the inbound edge of Callisto's geometric shadow, where the discrepancies between the observed $B_x > 0$ feature of the quasi-dipolar core region and the hybrid model are greatest. Had this M-like feature not been present, the modeled B_x component would have agreed with the observed B_x nearly perfectly through the entire core region of Callisto's wake, especially along the two slightly shifted trajectories (green and orange). Of our multiple simulation runs for the C10 flyby, none were able to reproduce this M-like magnetic field signature. Therefore, the M-like perturbation in B_x and B_z may have been magnetospheric in origin and hence unrelated to Callisto's local plasma interaction.

Alternatively, this M-structure in B_x and B_z could be associated with the onset of a narrow density filament of enhanced ionospheric outflow which would become more pronounced in Callisto's intermediate wake (see Figure 2d and discussion in section 4.1). This interpretation is supported by the approximate doubling of the measured electron density at the same time (highlighted in turquoise in Figure 3, fifth panel). The location of such a channel would be highly sensitive to incident flow conditions, as shown for Saturn's moon Titan by *Feyerabend et al.* [2015]. However, although far more pronounced channels of ionospheric outflow have been observed at Titan, the Cassini spacecraft has not detected similarly strong magnetic features associated with such outflow signatures [*Coates et al.*, 2012; *Simon et al.*, 2007, 2014].

During the C10 flyby, Galileo detected an enhancement and subsequent decrease in the measured magnetic field magnitude |**B**| (see Figure 3). The observed magnetic field magnitude shows qualitatively similar features as the B_y component, including the nearly featureless inbound segment and a bipolar magnetic perturbation within Callisto's geometric shadow. The similarities of B_y and |**B**| are expected, as $B_{y,0}$ was the strongest component of the background field during C10.

In analogy to the strong impact of the *observed* B_y on the *observed* |**B**|, the *modeled* B_y largely determines the structure of the *modeled* |**B**|. The pure dipole model (blue) is able to reproduce the observed |**B**| until near 00:20 but does not show a depletion of |**B**| after this time. The hybrid model (red, green, and orange) qualitatively matches the bipolar perturbation detected by Galileo starting after 00:15 and also explains its monotonic return to |**B₀**| starting near the edge of Callisto's geometric shadow.

The two-dimensional structure of |**B**| in the $z = 0$ plane is displayed in Figure 4e. The magnetospheric field piles up at Callisto's ramside (visible in dark blue), whereas above the moon's magnetic poles, the antialignment of **M**ind and **B₀** generates a reduction in |**B**| (light yellow). The magnetospheric plasma transports these regions of reduced |**B**| toward downstream, yielding a diffuse reduction of the total field in Callisto's wake that was detected during C10.

4.2.4. Electron Number Density

Measurements of the electron number density n_e during the C10 flyby are presented on a logarithmic scale in Figure 3 (fifth panel) in black. These data were obtained by the plasma wave instrument on Galileo and were extracted from Figure 3 in *Gurnett et al.* [2000]. The measurements contain a gap in the electron density between 00:25 and 00:27, where the data were extrapolated (black dashed line). No further electron density data from Galileo have been published for the inbound segment (prior to 00:08) or the outbound segment (after 00:30) of the C10 encounter.

Starting around 00:08, Galileo detected an enhancement of the electron density associated with cold plasma outflow from Callisto. The region of enhanced n_e formed a plateau-like feature with electron density values that hovered around 100 cm⁻³ between 00:10 and 00:23 (Figure 3). That is, the measured electron number density was increased by 3–4 orders of magnitude compared to typical values of the background plasma number density near Callisto [*Kivelson et al.*, 2004]. The plateau was followed by a gradual decrease to values below $n_e \approx 1$ cm⁻³ which began near 00:23 as the spacecraft exited Callisto's geometric shadow.

Hybrid model results for the electron density are again displayed in red, green, and orange in Figure 3. Along all three trajectories, the modeled electron density shows a plateau-like structure, the shape and magnitude of which are consistent with Galileo observations. The agreement is best along the actual C10 trajectory (red) and the trajectory shifted by 0.1 R_C toward Callisto (green), as the electron density value along both trajectories remains around 100 cm⁻³ within the plateau region. The trajectory shifted even closer to Callisto (orange) passes through a denser part of the moon's ionosphere and shows a pronounced bulge around 00:20 that was not visible in Galileo data. This bulge begins just before C/A and persists until exiting Callisto's geometric shadow.
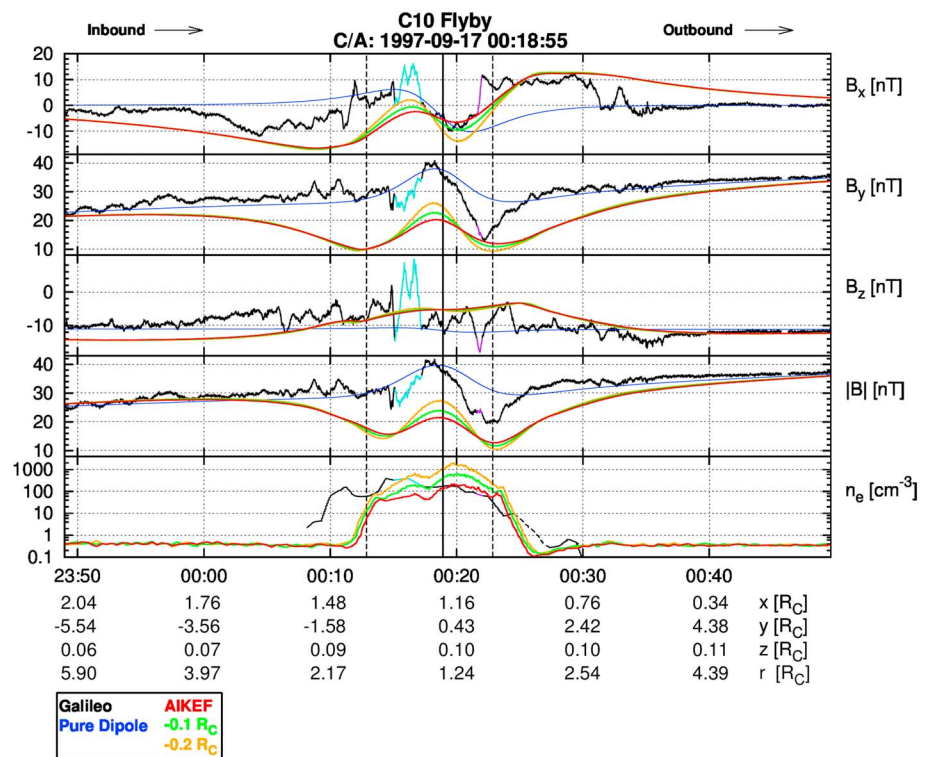
Figure 5. Same as Figure 3 but for the hybrid simulation with the magnetospheric flow vector $\mathbf{u}_0$ rotated by 20° toward Jupiter. Dashed vertical black lines represent the location of Callisto's geometric shadow, and the solid vertical line marks the time of closest approach. Galileo spacecraft data are in black, and in blue is the pure dipole approximation. The hybrid results are in red for the C10 trajectory, in green for the trajectory shifted by $-0.1\,R_C$, and in orange for the trajectory shifted by $-0.2\,R_C$. The (turquoise) M-like perturbation feature and the (purple) rotational discontinuity are discussed in the text.

The modeled plateau-like region in n_e extends approximately $2\,R_C$ along each trajectory, while the measured plateau region was slightly more extended by approximately $0.6\,R_C$ into the Jupiter-averted ($y < 0$) hemisphere. It is interesting to note here that the deviation between modeled and observed B_y also occurs in this region (see section 4.2.2) but is much more extended into the Jupiter-averted hemisphere. However, the electron density in the outbound segment of the flyby is modeled accurately. This is especially evident as the gradual decrease generated by the hybrid simulation is in agreement with Galileo data from Callisto's Jupiter-facing hemisphere. As can be seen from Figure 2d, the plateau-like region in n_e was associated with Galileo's passage through the narrow tail of escaping ionospheric plasma downstream of Callisto.

To explore the cause of the discrepancy between the modeled and measured width of the electron density enhancement during the inbound region of C10, a local atmospheric inhomogeneity in Callisto's Jupiter-averted hemisphere was introduced into the hybrid model. Given the lack of observations of Callisto's atmosphere and ionosphere at the time of C10, multiple simulations with different "strengths" and extensions of this inhomogeneity were performed. In order to reproduce the increased width of the observed electron density enhancement, the atmospheric density in the Jupiter-averted hemisphere must locally exceed the highest density value ever postulated for Callisto (on the order of $1 \cdot 10^{10}\,\mathrm{cm}^{-3}$, cf. *Kliore et al.* [2002] or *Liang et al.* [2005]) by a factor of 10. In other words, although a local plume-like source would, in principle, slightly improve agreement between the modeled and measured electron density enhancements, we certainly *do not* dare to postulate the existence of such a source based only on the electron density observations from a single flyby.

4.3. Robustness of Modeled Results for the C10 Flyby

Tentative analysis of Galileo plasma data provide hints that the upstream flow near Callisto may have a nonnegligible deviation from the corotation direction [*Bagenal et al.*, 2016]. To investigate the impact of a nonazimuthal flow component on Callisto's plasma interaction during C10, we conducted a series of simulations using the *direction* of the upstream flow velocity $\mathbf{u}_0$ as a free parameter. As an example, Figure 5 shows hybrid model results with upstream flow offset 20° from corotation (see discussion in section 3). In black are

the Galileo magnetic field and electron density measurements, with the pure dipole model results in blue and the hybrid model results in red, green, and orange, as similar to Figure 3.

For each component of the magnetic field in Figure 5, the features obtained for $\mathbf{u}_0$ aligned with corotation (see Figures 3 and 4) are visible in this simulation as well. Most notably, the alternating signs of the B_x perturbations (indicating Callisto's Alfvén wings and the wakeside core region dominated by the quasi-dipolar induced field), the bipolar B_y perturbation within Callisto's geometric shadow, and the plateau-like region in B_z are still visible for all three trajectories shown. Overall, rotating the incident flow by 20° toward Jupiter resulted only in a minor quantitative impact on the model results. Using a rotation of the flow vector away from Jupiter also produced similar results.

The electron density structure of the simulation with the nonazimuthal flow velocity is also displayed in Figure 5. As with the previous simulation, the plateau of enhanced electron density (approximately 100 cm^{-3}), lasting for about 2 R_C along the trajectory, is still visible. The similarities between the results of both simulations suggest a strong level of robustness of the modeled C10 magnetic field and density signatures against changes of the incident flow direction, at least as long as the upstream conditions are stationary on the length and time scales of the encounter.

In addition to induction within Callisto's subsurface ocean, the magnetic field near the moon may also be affected by currents induced within its transient, time-varying ionosphere [*Kliore et al.*, 2002] to a minor degree. However, based on their analysis of C3 and C9 data, *Zimmer et al.* [2000] found the ionospheric induction effect to be negligible compared to the inductive response of the ocean. Due to the unknown upstream conditions during the C10 flyby, it is not feasible to use magnetic field data from C10 to impose further constraints on the inductive response of the ionosphere.

5. Summary and Concluding Remarks

This study has presented a comprehensive analysis of magnetic field and plasma data from the Galileo C10 flyby of Callisto on 17 September 1997 with a C/A altitude of 535 km (0.22 R_C). During the flyby, Galileo passed through Callisto's plasma wake while moving toward Jupiter in the moon's equatorial plane.

To constrain the contributions of plasma interaction and magnetic induction signals from Callisto's subsurface ocean to the observed interaction features, we have compared in situ data from Galileo against hybrid (kinetic ions and fluid electrons) simulations of Callisto's plasma environment. A hybrid approach is necessary since pickup ions from Callisto can have gyroradii nearly 10 times larger than the moon's radius [*Kivelson et al.*, 2004; *Liuzzo et al.*, 2015]. For the first time, we have successfully modeled Callisto's magnetic environment during a flyby where the moon's plasma interaction and the induced magnetic field both made significant contributions to the observed interaction signatures. We have identified a region downstream of Callisto where a clear discrimination between the induction signal and the structures associated with the plasma interaction is feasible. This study has determined the following:

1. Field line draping and the induced dipole both contributed to the magnetic signatures detected during the C10 flyby, with each effect dominating in different regions of the near-Callisto environment. The magnetic perturbations observed beyond $y \approx \pm 2\, R_C$ were associated with the Alfvén wings, mainly generated by the magnetospheric interaction with Callisto's ionosphere. Closer to the moon's surface and in its wake, the induced dipole dominated over the plasma interaction in a core region directly downstream of Callisto. In the moon's Jupiter-facing hemisphere, Galileo detected a rotational discontinuity in the magnetic field, clearly separating these two distinct regimes of Callisto's magnetic environment. At the moon's ramside hemisphere, the induced dipole was completely obscured by magnetospheric field line draping and pileup. That is, there was no quasi-dipolar core region upstream of Callisto.

2. The AIKEF hybrid model was able to explain numerous key features of Callisto's magnetic and plasma environment during C10. These included the observed sequence of Alfvén wing and dipole signatures in B_x, the plateau-like enhancement of B_z, and a narrow region of escaping ionospheric plasma downstream of Callisto. Discrepancies between the model and observations (mainly visible in B_y) were possibly associated with small-scale magnetospheric variations as well as the poorly constrained parameters of Callisto's atmosphere and the ambient magnetospheric plasma during the encounter.

3. Even when the plasma currents near Callisto are strong, the induced dipole leaves a clear imprint in the observed magnetic field. However, in contrast to Europa [e.g., *Kurth et al.*, 2001], a characterization of the
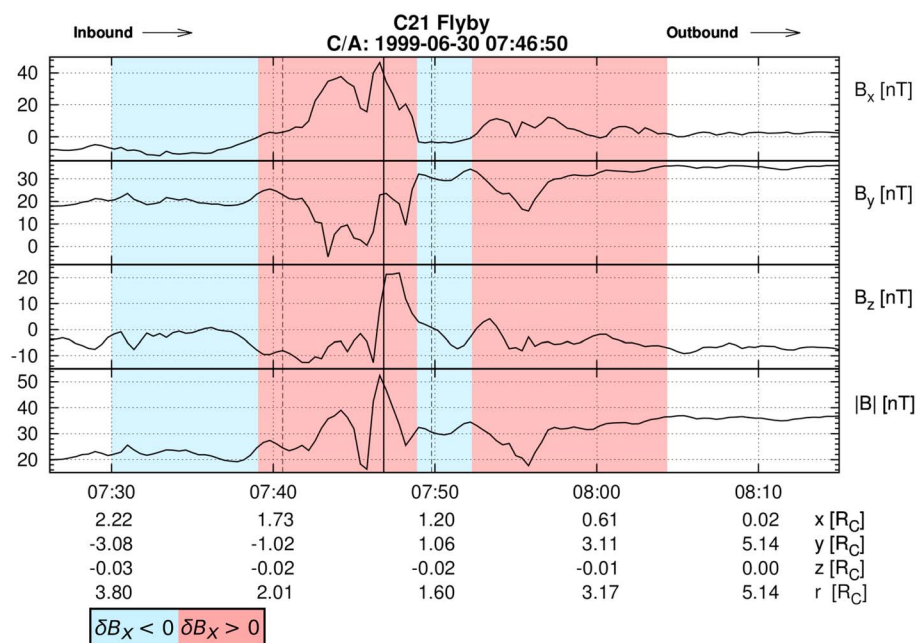
Figure 6. Galileo magnetic field data for the C21 flyby of Callisto on 30 June 1999. Black vertical lines represent the location of (dashed) Callisto's geometric shadow and (solid) closest approach of Galileo. Data collected during the flyby are presented in black. Shaded regions correspond to regions of (blue) $\delta B_x < 0$ and (red) $\delta B_x > 0$ perturbations.

incident flow conditions at Callisto is not available on a flyby-to-flyby basis. In combination with the aforementioned uncertainties in the properties of Callisto's atmosphere, this makes it difficult to determine the degree to which the induced dipole is deformed and obscured by currents associated with the moon's plasma interaction. For this reason, Callisto flyby data collected within the Jovian current sheet cannot readily be used to further constrain the induced dipole strength and hence the properties (conductivity, thickness, and depth) of Callisto's subsurface ocean, apart from confirming its mere existence. A comprehensive characterization of Callisto's atmosphere and the upstream plasma during the respective flyby would be required to refine the existing constraints [see *Kivelson et al.*, 1999; *Zimmer et al.*, 2000] on the properties of the ocean.

4. The upcoming JUICE (JUpiter ICy moon Explorer) mission will collect magnetic field data near Callisto to further understand properties of the moon's subsurface ocean. However, our analysis of magnetic field data from C10 asserts that to improve the existing constraints on the ocean with future flyby data, it is imperative to encounter Callisto far outside of Jupiter's current sheet where the induction signal clearly dominates over perturbations generated by plasma currents.

5. The Galileo C10 flyby occurred when Callisto's wakeside hemisphere (i.e., the leading hemisphere) was sunlit. While *Kliore et al.* [2002] suggested that the ramside of Callisto must be sunlit for an appreciable ionosphere to be present, the 3–4 orders of magnitude density enhancement observed in Callisto's wake, along with the strong magnetic draping signatures (due to ionospheric current systems), imply that Callisto must have possessed an appreciable global ionosphere at the time of C10. The quantitative agreement between the hybrid model and electron density data from Galileo affirms that the ionosphere representation in the hybrid model is indeed accurate. The presence of a dense ionosphere during C10 is further substantiated by the fact that the hybrid model of *Lindkvist et al.* [2015], which neglected the contribution of Callisto's ionosphere to its plasma interaction, did not produce any noticeable draping signatures in B_x along the C10 trajectory [see *Lindkvist et al.*, 2015, Figure 10]. That model was also unable to generate the wakeside density increase by 3–4 orders of magnitude that was detected by Galileo [see *Lindkvist et al.*, 2015, Figure 7].

Similar to structures observed during the C10 encounter, signatures of magnetic field line draping and a quasi-dipolar core region downstream of Callisto may have also been detected during the C21 flyby on 30 June 1999. Figure 6 shows magnetic field data obtained by the Galileo spacecraft during this flyby, the trajectory of which was highly similar to that of C10. Colored areas correspond to regions potentially dominated by magnetic field line draping or by the induced dipole, as indicated by the sign of δB_x. The sequence of the

alternating δB_x perturbations was the same as the sequence observed during the C10 flyby (see Figure 4a). However, the peak perturbation of $\delta B_x \approx 50$ nT during C21 is, at first glance, an atypically strong magnetic response compared to the C10 data and is not predicted by available models of Callisto's magnetic environment. A quantitative understanding of the magnetic signatures observed during C21 is therefore the subject of our future work.

References

Bagenal, F., R. J. Wilson, S. Siler, W. R. Paterson, and W. S. Kurth (2016), Survey of Galileo plasma observations in Jupiter's plasma sheet, *J. Geophys. Res. Planets*, *121*(5), 871–894.

Carlson, R. W. (1999), A tenuous carbon dioxide atmosphere on Jupiter's moon Callisto, *Science*, *283*(5403), 820–821, doi:10.1126/science.283.5403.820.

Coates, A. J., et al. (2012), Cassini in Titan's tail: CAPS observations of plasma escape, *J. Geophys. Res.*, *117*, A05324, doi:10.1029/2012JA017595.

Cunningham, N. J., J. R. Spencer, P. D. Feldman, D. F. Strobel, K. France, and S. N. Osterman (2015), Detection of Callisto's oxygen atmosphere with the Hubble Space Telescope, *Icarus*, *254*, 178–189.

Feyerabend, M., S. Simon, U. Motschmann, and L. Liuzzo (2015), Filamented ion tail structures at Titan: A hybrid simulation study, *Planet. Space Sci.*, *117*, 362–376.

Gurnett, D. A., A. M. Persoon, W. S. Kurth, A. Roux, and S. J. Bolton (2000), Plasma densities in the vicinity of Callisto from Galileo plasma wave observations, *Geophys. Res. Lett.*, *27*(13), 1867–1870, doi:10.1029/2000GL003751.

Khurana, K. K., M. G. Kivelson, D. J. Stevenson, G. Schubert, C. T. Russell, R. J. Walker, and C. Polanskey (1998), Induced magnetic fields as evidence for subsurface oceans in Europa and Callisto, *Nature*, *395*(6704), 777–780, doi:10.1038/27394.

Kivelson, M. G., K. K. Khurana, D. J. Stevenson, L. Bennett, S. Joy, C. T. Russell, R. J. Walker, C. Zimmer, and C. Polanskey (1999), Europa and Callisto: Induced or intrinsic fields in a periodically varying plasma environment, *J. Geophys. Res.*, *104*(A3), 4609–4626, doi:10.1029/1998JA900095.

Kivelson, M. G., F. Bagenal, W. S. Kurth, F. M. Neubauer, C. Paranicas, and J. Saur (2004), Magnetospheric interactions with satellites, in *Jupiter. The Planet, Satellites and Magnetosphere*, edited by M. G. Kivelson et al., pp. 513–536, Cambridge Univ. Press, Cambridge, U. K.

Kliore, A. J., A. Anabtawi, R. G. Herrera, S. W. Asmar, A. F. Nagy, D. P. Hinson, and F. M. Flasar (2002), Ionosphere of Callisto from Galileo radio occultation observations, *J. Geophys. Res.*, *107*, 1407, doi:10.1029/2002JA009365.

Kriegel, H., S. Simon, P. Meier, U. Motschmann, J. Saur, A. Wennmacher, D. F. Strobel, and M. K. Dougherty (2014), Ion densities and magnetic signatures of dust pick-up at Enceladus, *J. Geophys. Res. Space Physics*, *119*(4), 2740–2774, doi:10.1002/2013JA019440.

Kurth, W. S., D. A. Gurnett, A. M. Persoon, A. Roux, S. J. Bolton, and C. J. Alexander (2001), The plasma wave environment of Europa, *Planet. Space Sci.*, *49*, 345–363, doi:10.1016/S0032-0633(00)00156-2.

Liang, M.-C., B. F. Lane, R. T. Pappalardo, M. Allen, and Y. L. Yung (2005), Atmosphere of Callisto, *J. Geophys. Res.*, *110*, E02003, doi:10.1029/2004JE002322.

Lindkvist, J., M. Holmström, K. Khurana, S. Fatemi, and S. Barabash (2015), Callisto plasma interactions: Hybrid modeling including induction by a subsurface ocean, *J. Geophys. Res. Space Physics*, *120*, 4877–4889, doi:10.1002/2015JA021212.

Liuzzo, L., M. Feyerabend, S. Simon, and U. Motschmann (2015), The impact of Callisto's atmosphere on its plasma interaction with the Jovian magnetosphere, *J. Geophys. Res. Space Physics*, *120*(11), 9401–9427.

Müller, J., S. Simon, U. Motschmann, J. Schüle, K. Glassmeier, and G. J. Pringle (2011), A.I.K.E.F.: Adaptive hybrid model for space plasma simulations, *Comput. Phys. Commun.*, *182*(4), 946–966, doi:10.1016/j.cpc.2010.12.033.

Neubauer, F. M. (1980), Nonlinear standing Alfven wave current system at Io: Theory, *J. Geophys. Res.*, *85*, 1171–1178, doi:10.1029/JA085iA03p01171.

Neubauer, F. M. (1998), The sub-Alfvénic interaction of the Galilean satellites with the Jovian magnetosphere, *J. Geophys. Res.*, *103*, 19,843–19,866, doi:10.1029/97JE03370.

Neubauer, F. M. (1999), Alfvén wings and electromagnetic induction in the interiors: Europa and Callisto, *J. Geophys. Res.*, *104*, 28,671–28,684, doi:10.1029/1999JA900217.

Richards, P. C., J. A. Fennelly, and D. G. Torr (1994), EUVAC: A solar EUV flux model for aeronomic calculations, *J. Geophys. Res.*, *99*, 8981–8992.

Rubin, M., et al. (2015), Self-consistent multifluid MHD simulations of Europa's exospheric interaction with Jupiter's magnetosphere, *J. Geophys. Res. Space Physics*, *120*(5), 3503–3524.

Seufert, M. (2012), Callisto: Induction signals, atmosphere and plasma interaction, PhD thesis, Univ. zu Köln.

Seufert, M., J. Saur, and F. M. Neubauer (2011), Multi-frequency electromagnetic sounding of the Galilean moons, *Icarus*, *214*(2), 477–494, doi:10.1016/j.icarus.2011.03.017.

Simon, S., G. Kleindienst, A. Boesswetter, T. Bagdonat, U. Motschmann, K.-H. Glassmeier, J. Schuele, C. Bertucci, and M. K. Dougherty (2007), Hybrid simulation of Titan's magnetic field signature during the Cassini T9 flyby, *Geophys. Res. Lett.*, *34*(L24S08), doi:10.1029/2007GL029967.

Simon, S., J. Saur, H. Kriegel, F. Neubauer, U. Motschmann, and M. Dougherty (2011), Influence of negatively charged plume grains and hemisphere coupling currents on the structure of Enceladus' Alfvén wings: Analytical modelling of Cassini magnetometer observations, *J. Geophys. Res.*, *116*(A4), A04221, doi:10.1029/2010JA016338.

Simon, S., F. M. Neubauer, A. Wennmacher, and M. K. Dougherty (2014), Variability of Titan's induced magnetotail: Cassini magnetometer observations, *J. Geophys. Res.*, *119*(3), 2024–2037.

Simon, S., E. Roussos, and C. Paty (2015), The interaction between Saturn's moons and their plasma environments, *Phys. Rep.*, *602*, 1–65.

Sonnerup, B. U. O., and L. J. Cahill (1967), Magnetopause structure and attitude from Explorer 12 observations, *J. Geophys. Res.*, *72*(1), 171–183, doi:10.1029/JZ072i001p00171.

Strobel, D. F., J. Saur, P. D. Feldman, and M. A. McGrath (2002), Hubble Space Telescope Space Telescope Imaging Spectrograph search for an atmosphere on Callisto: A Jovian unipolar inductor, *Astrophys. J.*, *581*(1), L51–L54, doi:10.1086/345803.

Vorburger, A., P. Wurz, H. Lammer, S. Barabash, and O. Mousis (2015), Monte-Carlo simulation of Callisto's exosphere, *Icarus*, *262*, 14–29.

Zimmer, C., K. K. Khurana, and M. G. Kivelson (2000), Subsurface oceans on Europa and Callisto: Constraints from Galileo magnetometer observations, *Icarus*, *147*(2), 329–347, doi:10.1006/icar.2000.6456.